

Metasomatism, titanian acmite, and alkali amphiboles in lithic-wacke inclusions within the Coyote Peak diatreme, Humboldt County, California

GERALD K. CZAMANSKE AND STEVEN A. ATKIN¹

U.S. Geological Survey
345 Middlefield Road, Menlo Park, California 94025

Abstract

Lithic-wacke inclusions within the alkalic ultramafic diatreme at Coyote Peak record a remarkable history of metasomatism and crystal growth. Dominant metasomatic changes were loss of Si from the inclusions and mass influx of K, due to an unusually high K activity in the ultramafic host. Reaction with K converted much of the clay, quartz, and lithic fraction of the lithic wacke into microcline and exchanged Na from abundant clastic albite.

Sodium released from albite: (1) combined with Ti and Fe to form myriads of acmite crystals, many of which are strongly zoned with cores unusually rich in titanium; (2) combined with Ti, Fe, Mg, and Ca to form alkali amphiboles, which are zoned from fluorrichterite cores to unusual titanian-arfvedsonite rims; and (3) formed a late-stage zeolite similar to natrolite. The sequence of ferromagnesian phases is interpreted to have been controlled partly by falling temperature, but dominantly by falling f_{O_2} , as the oxidized sedimentary assemblage equilibrated with the reduced ultramafic melt.

Preservation of primary sedimentary textures to within a few millimeters of the lithic-wacke/ultramafic interface in zoned inclusions and strong zonation between the cores and rims of individual phases suggest that recrystallization and chemical exchange were of short duration because of rapid emplacement and cooling of the diatreme at shallow depth.

Introduction

An alkalic, ultramafic diatreme 260 by 500 m in outcrop area penetrates a lithic-wacke sandstone sequence of the Franciscan assemblage, 20 km SE of Orick, at Coyote Peak, Humboldt County, California. Rocks comprising the diatreme may be conveniently subdivided into uncontaminated and contaminated variants, based on SiO_2 content, color, mineralogy, the character of contained clots, and abundance of inclusions. Poor exposures do not permit these variants to be mapped separately. Uncontaminated rocks comprise two distinct assemblages, each containing phenocrysts of subhedral to rounded olivine (to 2 mm; reverse zoned from Fe_{80} to Fe_{82} ; $NiO = 0.04$, $MnO = 0.4$ and $CaO = 0.5$ wt.%) and anhedral titanomagnetite (zoned from 13 to 9 wt.% TiO_2 and from 5 to 4 wt.% MgO). Groundmass phases in the most pristine assemblage are phlogopite ($X_{phlog} = 0.8$ to 0.9), melilite $[(Ca_2Fe)_{12}(Ca_2Mg)_{57}(CaNaAl)_{31}]$, nepheline ($Ne_{75}Ks_{25}$), magnetite ($TiO_2 < 7$ and $MgO < 2$ wt.%), perovskite, apatite, sodalite, and poikilitic garnet containing up to 16 wt.% TiO_2 . A second assemblage, characterized by coronas of pyroxene plus phlogopite around olivine, contains essential augite ($Wo_{50}En_{43}Fs_7$) and nepheline ($Ne_{75}Ks_{25}$) and lacks melilite. Study of many thin sections shows the assemblages to be related to one another by an evolutionary,

reaction process. Rocks characterized by both mineral assemblages are black; they also contain discrete coarse-grained clots (to 6 cm) composed of phlogopite, garnet (zoned from 12 to 2 wt.% TiO_2), minor sodalite and pectolite, pyrrhotite, and at least five K-Fe and Na-Fe sulfide minerals (Czamanske et al., 1979, 1980, and 1981; Erd and Czamanske, 1983). Considering mineral assemblages, pristine rock at Coyote Peak might best be termed modlibovite (Scheumann, 1913). Contaminated rocks are greenish in color, but essentially are composed of the reacted mineral assemblage found in the uncontaminated rocks. Also present are pectolite and natrolite, and a feathery garnet that is less Ti-rich (8 to 1 wt.%) and more aluminous (2.6 to 6 wt.%) than garnet in uncontaminated rocks. Contaminated rocks contain a totally different type of zeolitic clot, rich in natrolite and containing acmite, alkali amphibole, biotite (X_{phlog} to 0.44), titanite, and barytolamprophyllite (8.8 to 26 wt.% BaO).

The contaminated rocks contain reacted fragments of mudstone, as well as rounded inclusions of lithic wacke picked up from the Franciscan assemblage at the time of emplacement. These lithic-wacke fragments have undergone substantial chemical exchange with the diatreme, including extreme potassic metasomatism. Small (less than 3-cm diameter) inclusions, which are uniformly pale gray green, initially were thought to represent fine-grained potassic igneous rocks (Czamanske et al., 1977). Larger (diameter 6–10 cm) fragments commonly have brown cores and distinct gray-green rims, 8 to 12 mm thick, that closely

¹ Present address: Molycorp, Inc., Questa Division, P. O. Box 469, Questa, New Mexico 87556.

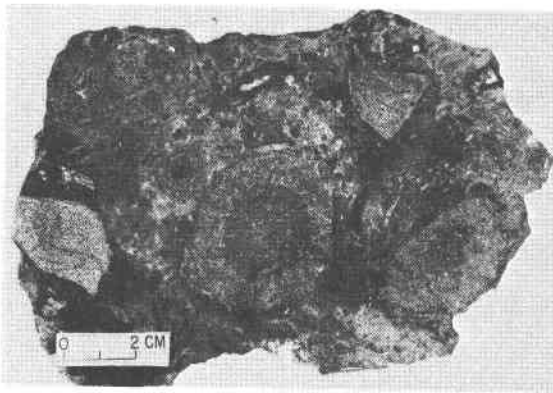


Fig. 1. Specimen from the Coyote Peak diatreme containing four lithic-wacke inclusions. Inclusions on left and upper right are typical of the more uniformly altered, small inclusions (e.g., sample CYP8); the two larger, rounded inclusions show distinct core and rim components.

resemble in color and texture the smaller, more uniformly altered inclusions (Fig. 1).

Due to the extreme disparity in composition between the ultramafic host and the included lithic-wacke fragments (Table 1), this study provides a special opportunity to describe pronounced metasomatic exchange. Resulting mineral assemblages contain titanian acmite and alkali amphiboles of unusual interest.

Petrography

We selected eight samples for study, including: (1) uniformly altered small inclusions (CYP8 and 103); (2) a medium-size inclusion (CYP52); (3) large inclusions with distinct core and rim alteration facies (CYP7, 101, 102, and 178); and (4) a sample of lithic-wacke country rock (CYP4) collected from a surface outcrop a few meters beyond the diatreme contact (which is nowhere exposed). In addition, sample CYP5 was selected as representative of the uncontaminated ultramafic melt.

The country rock (CYP4) is a light-tan well-indurated massive fine- to medium-grained moderately sorted lithic wacke. By volume it is composed of quartz (20%); albite (10%; $Ab_{99.6}$); lithic fragments, including shale, chert, and minor volcanic- and metamorphic-rock fragments (40%); and a turbid clay-rich matrix (25%). Altered biotite, chlorite, and muscovite (total, approximately 5%) are also present (Table 6). Franciscan graywacke of the northern Coast Ranges of California is noted for the absence of potassium feldspar (Bailey et al., 1964), and no potassium feldspar was seen in sample CYP4. Scattered dark-gray shale chips give the sandstone a salt-and-pepper appearance and, along with other elongate clasts, create rude sedimentary layering.

The earliest stages of lithic-wacke alteration cannot be documented because pristine lithic wacke was not found in the cores of even the largest included fragments and the

contacts of the diatreme are not exposed. The mineral assemblage in the brown cores of the largest inclusion (sample CYP101) comprises dominant compositionally intermediate alkali feldspar, a stilpnomelane-like phase (see below), and minor quartz. Relic clastic grains of quartz and partially exchanged alkali feldspar preserve sedimentary bedding. Interstices between relic clasts are filled with turbid intermediate alkali feldspar, similar in composition to that of the partially exchanged clasts. The stilpnomelane-like phase (pleochroic in amber hues) occurs as xenomorphic bundles of platy or acicular grains (maximum 0.5 mm) scattered throughout the matrix. This phase may also occur, however, as delicate plumes that have nucleated along the margins of, and appear partly to replace clastic quartz grains (Fig. 2A).

Boundaries between the brown cores and gray-green rims of larger inclusions are distinct (Fig. 1); this color change apparently reflects the presence of the stilpnomelane-like phase in the core assemblage and of acmite and alkali amphibole in the rim assemblage. The rims of the larger inclusions are mineralogically essentially identical to the more homogeneous, smaller inclusions and consist of titanian-acmite, alkali amphibole, alkali feldspar (which grades to K-rich microcline as the contact with the host diatreme is approached), a natrolite-like zeolite, a fibrous unidentified Ca-Na silicate, and rare wollastonite. The disappearance of the stilpnomelane-like phase at the core-rim boundary is abrupt, but there is no microscopic evidence for any singular reconstitution reaction. Feldspar compositions do not change abruptly at the core-rim boundary, and remnant clastic alkali-feldspar grains of intermediate composition may persist well into the rims. Feldspars become progressively less sodic toward the edge of a given inclusion, and individual grains are typically zoned, with rims that are enriched in K relative to their cores. Toward the interface with the matrix, feldspars in some larger zoned inclusions, and in most smaller inclusions, are thoroughly recrystallized into mosaics of xenoblastic to idioblastic grains of maximum microcline (as determined from its powder-diffraction pattern). Alkali feldspar may display turbid cores and clear rims where it contacts the natrolite-like zeolite (Figs. 2C and 2E). This development of a more nearly uniform, granoblastic texture obliterates all relic sedimentary features.

Titanian acmite first appears at the core-rim boundary of large inclusions, where chains of acmite grains, 20 to 60 μm on an edge, commonly surround relic feldspar and quartz grains (Fig. 2B). As the rim is traversed toward the inclusion/ultramafic interface, acmite becomes widely distributed and ever-larger idioblastic grains or clusters of idioblastic crystals are found, although fine grains persist. The domain of alkali amphibole crystallization appears not to extend quite so far inward from the ultramafic/inclusion interface as that of acmite, and alkali amphibole grains are always larger than associated acmite crystals. The latter relation is particularly conspicuous where there has been maximum crystal growth, as found in small inclusions; there, large zoned idioblastic acmite crystals (rarely 1.0 mm

Table 1. X-ray fluorescence analyses and CIPW norms for ultramafic host rock, lithic-wacke country rock, and metasomatized lithic wacke, Coyote Peak, California. (Bi-Shia King, analyst).

	Average Franciscan graywacke*	Lithic-wacke country rock CYP4	Metasomatized lithic wacke					Ultramafic host CYP5
			Core CYP101A	Rim CYP101B	Rim CYP102B	Small inclusions (2x3 cm) CYP103 CYP8		
SiO ₂	67.5	70.62	61.02	61.98	60.35	61.05	61.07	33.86
Al ₂ O ₃	13.5	13.11	16.18	15.93	15.48	14.74	15.35	9.41
TiO ₂	0.5	0.60	0.54	0.48	0.53	0.42	0.42	3.14
Fe ₂ O ₃	1.2	1.59	1.84	1.71	1.97	3.12	2.65	7.89
FeO	3.0	3.28	1.75	1.52	2.17	0.84	0.47	6.41
MnO	0.1	0.06	0.06	0.06	0.06	0.05	0.03	0.31
MgO	2.2	1.82	1.28	1.48	1.93	1.83	1.25	9.42
CaO	2.4	0.38	1.78	1.62	2.76	0.33	1.48	19.09
BaO	—	0.04	0.12	0.08	0.08	0.08	0.08	0.15
Na ₂ O	3.6	4.35	4.34	2.98	2.72	3.59	3.46	4.75
K ₂ O	1.7	0.82	7.79	11.08	10.96	12.22	11.77	1.58
P ₂ O ₅	0.1	0.13	0.10	0.11	0.12	0.03	0.02	1.98
H ₂ O ₊	2.5	2.14	1.38	0.49	0.45	0.83	0.93	0.61
H ₂ O ⁻	0.4	0.38	1.20	0.20	0.22	0.24	0.29	0.04
F	—	0.04	0.05	0.13	0.10	0.10	0.06	0.19
Total	98.70	99.36	99.43	99.85	99.90	99.47	99.33	98.83**
Q	—	38.9	2.2	—	—	—	—	—
C	—	5.2	—	—	—	—	—	—
Or	—	5.0	47.3	65.9	65.2	73.3	70.9	—
Ab	—	37.9	37.7	20.3	13.8	7.9	11.2	—
An	—	—	1.7	—	—	—	—	1.7
Ne	—	—	—	—	2.7	—	1.4	19.8
Ac	—	—	—	4.4	3.9	9.2	7.8	—
Ns	—	—	—	—	—	2.9	1.7	—
Mg-Di	—	—	2.7	3.3	6.5	0.3	5.0	18.3
Fe-Di	—	—	0.6	1.4	3.1	0.1	0.3	—
Hy	—	8.6	2.6	—	—	3.9	—	—
Ol	—	—	—	2.4	2.1	1.1	0.7	10.5
Mt	—	2.4	2.7	0.3	0.9	0.0	0.0	11.1
Il	—	1.2	1.1	0.9	1.0	0.8	0.8	6.0
Salic	—	87.0	89.0	86.3	81.7	81.3	83.4	29.8***
Femic	—	12.9	10.9	13.6	18.2	18.7	16.5	69.7***

*Average of 21 Franciscan graywacke sandstone analyses from samples collected throughout the section (Bailey *et al.*, 1964, Table 2, p. 34).

**Also: CO₂,0.18; Cl,0.50; S,0.42; Sr,0.24; and ZrO₂,0.09.

***Including: Ap,4.7; Cc,0.4; Cs,17.5; Hl,0.8; Hm,0.3; Lc,7.3; Pr,0.8; and Z,0.1.

long, with dark- to olive-green pleochroic cores and colorless nonpleochroic rims) or acmite-crystal aggregates and larger zoned xenoblastic alkali-amphibole grains (maximum 1.25 mm across) occur as disseminated porphyroblasts in a granoblastic matrix (Figs. 2D and 2E). Where best developed in small inclusions, alkali amphibole most commonly occurs as irregular grains (Fig. 2D) that can be taken at first glance for biotite; it has unusual pleochroism with predominant light-tan to lilac cores and irregular olive-green to purple "rims." Highly serrate edges of am-

phibole grains appear to result from impingement on small turbid groundmass patches or acmite crystals.

Relations between acmite and alkali amphibole are difficult to establish. Neither phase shows any clear indication of instability, with acmite often displaying sharp crystal faces and the serrate margins of amphibole grains appearing to be crisp growth features. Most acmite is not in association with amphibole, and no examples of fine acmite crystals including small patches of relic amphibole have been noted. On the other hand, many large amphibole

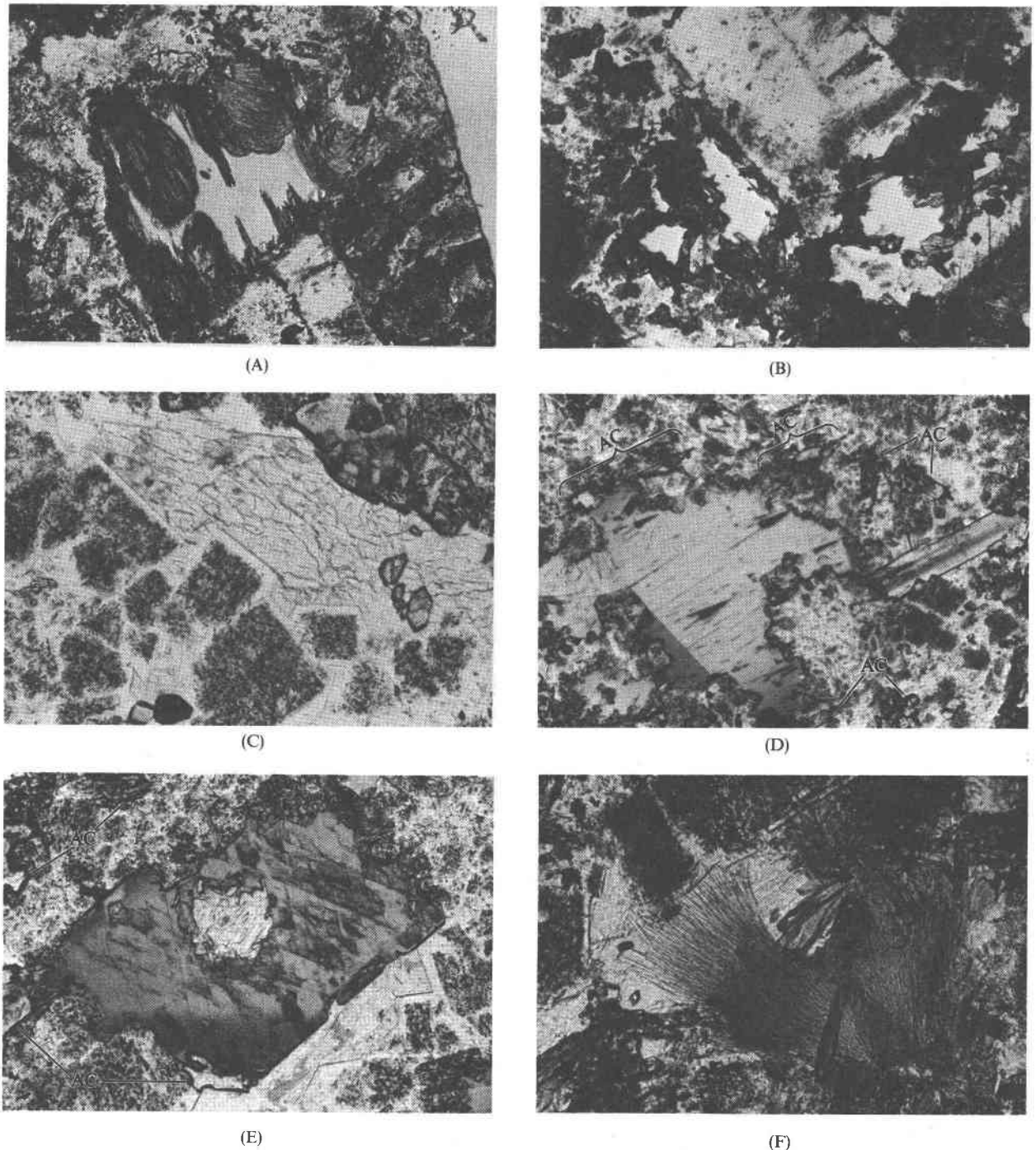


Fig. 2. (A) Replacement of a clastic quartz grain by the stilpnomelane-like phase (sample CYP7). Crystal at bottom center is alkali feldspar. Quartz grain is 0.25 mm across. (B) Alkali feldspar and quartz surrounded by finely crystalline acmite (dark, high relief) (sample CYP7). Feldspar grain is 0.37 mm wide. (C) Microcline, showing turbid cores and clear rims against interstitial, natrolite-like zeolite (sample CYP8). High-relief grains are acmite. It is 0.46 mm across the three large grains. (D) A typically anhedral large zoned alkali-amphibole grain in a matrix of microcline and acmite (AC) crystals (sample CYP8). Unusually large, strongly zoned acmite crystal (right center) is 0.58 mm long. (E) A large unusually well-formed zoned alkali-amphibole crystal (sample CYP8). Natrolite-like zeolite occurs both within the amphibole and between the grain and clear euhedral microcline rims. Amphibole crystal is 0.32 mm wide. Acmite grains, AC. (F) Fibrous unidentified Ca-Na silicate, intergrown with the natrolite-like zeolite on left and euhedral high relief acmite crystals just right of center (sample CYP52). Matrix is microcline and fine acmite crystals. Largest zeolite fibers are 0.36 mm long.

grains are in marginal contact with one or more acmite crystals or clusters of crystals (Fig. 2D and 2E). It is usually difficult to decide on textural grounds whether the acmite more commonly was being replaced by amphibole or was growing intimately upon it. This difficulty is illustrated by the two ragged acmite grains in the upper center and left side of Figure 2D. Three considerations suggest that in general crystallization of acmite preceded that of alkali amphibole: (1) Acmite crystallization extended farther into the larger inclusions, where fine crystals even coexist with quartz in zones marked by early stages of feldspar exchange (Fig. 2B). (2) Despite their relatively large size, amphiboles are not poikiloblastic, but typically have clear interiors (Figs. 2D and 2E), suggesting that they were able to assimilate or displace mineral phases, including acmite, until their growth ceased. (3) The patchy zoning at the amphibole rims (reflecting high Ti-content) often is developed in proximity to marginal acmite (e.g., Figs. 2D and 2E, bottom, center). Further commentary on acmite-amphibole relations is deferred to the discussion.

The natrolite-like zeolite (see below) is a common phase in the smaller inclusions, possibly less so in the rim assemblage of larger inclusions. It is interpreted to have been the last phase to crystallize because it typically occurs as interstitial aggregates scattered within a feldspar matrix (Figs. 2C and 2E). It appears to be in stable association with both acmite and alkali amphibole (Figs. 2C, 2E, and 2F). The fibrous Ca-Na silicate is less common and occurs as sheaves of radiating needles (maximum 0.5 mm long), often intergrown with the natrolite-like zeolite (Fig. 2F). This fibrous silicate is best developed in the smaller, more nearly homogeneous inclusions, but away from the inclusion/ultramafic interface.

Sample CYP7 is atypical in that overlapping rim alteration zones suggest that it was somehow exposed to two episodes of metasomatic alteration, perhaps by becoming uncoupled from its initial melt envelope. The only recognizable effects of this history are the presence of xenoblastic wollastonite grains in parts of the rim assemblage and the occurrence of enlarged grains of the stilpnomelane-like phase.

Between inclusions and the enveloping ultramafic host is an irregular monomineralic rind (maximum 0.3 mm thick) of light-green sodian augite ($\text{Wo}_{39}\text{En}_{36}\text{Fs}_{16}\text{Ac}_9$; Table 2) (augite is an essential phase within the alkalic ultramafic host). Some augite grains (maximum 0.25 mm cross) may extend from this rind as small tongues into the ultramafic host, while scattered augite grains occur within recrystallized lithic wacke adjacent to the augite rind and are commonly rimmed by titanian acmite or included within alkali amphibole. Ilmenite and titanite are minor phases within the recrystallized lithic wacke adjacent to the rind; magnetite and pyrite are rare.

Whole-rock chemistry

The analyses listed in Table 1 indicate the bulk chemical changes caused by metasomatism. Analyzed lithic-wacke

country rock (sample CYP4) and a representative sample of uncontaminated ultramafic host (sample CYP5; Morgan et al., 1985) are presumed to establish the chemistries of the rocks prior to metasomatism. The caution in this statement is based on two reservations: (1) the fragments included in the diatreme could originate from a stratigraphic interval which differs mineralogically and chemically from that presently exposed next to it, and (2) the lithic-wacke country rock may have been albitized by intrusion of the diatreme. We are unable to evaluate the first possibility, but consideration of data for "average" Franciscan graywacke (Table 1) suggests that our interpretations do not critically depend on proof of the equivalence between the included and host-rock lithic wacke. Whereas a careful sampling and analytical program could address the second possibility, we are unconvinced of the potential rewards of such a study. Analyses of two homogeneous small inclusions (samples CYP8 and 103), the rims of two larger inclusions (samples CYP101B and 102B), and the core zone of one of these inclusions (sample CYP101A) indicate the bulk chemical changes that accompany the several mineralogic changes just described. Most striking is the exceptional K_2O content of "fully altered" lithic wacke, which reaches 12 wt.%.

Comparison of the chemical analysis of sample CYP4 with an average of 21 analyses of Franciscan graywacke (Table 1) suggests that this sample may be a reasonable representative of the lithic wacke in the section as a whole and thus of the sedimentary sequence penetrated by the magma during emplacement of the diatreme. The higher alkali and lower CaO contents of sample CYP4 in comparison to those of "average" Franciscan graywacke reflect the presence of essentially pure albite, in contrast to feldspars elsewhere in the Franciscan assemblage, which range in composition from albite through oligoclase or andesine and have been reported locally to be as calcic as labradorite or bytownite.

Mineral chemistry

Mineral grains were analyzed in six Coyote Peak lithic-wacke samples, but most of the data presented here were obtained from samples CYP4, CYP8, CYP52, and CYP101. Mafic silicates in polished thin sections were analyzed with a three-channel ARL EMX-SM electron microprobe, using an accelerating potential of 15 kV and a sample current of 0.02 μA on benitoite. Elements were analyzed in the sequence Mg + K + Fe, Al + Si + Ti, F + Cl + Ca, and Na + Mn. All analyzed grains were photographed to allow relocation to be as precise as possible. Each reported analysis represents 6 to 12 points per grain or distinct portion of a zoned grain; each point was occupied for a count interval (about 10 seconds) fixed by beam-current termination. The selected amphibole, biotite, and pyroxene described by Czamanske and Wones (1973) were used as standards for most elements in the appropriate mineral species. Supplementary standards were Mn_2O_3 for Mn, TiO_2 for Ti, a synthetic fluorphlogopite for F (9.01 wt.%), a natural crocidolite for Na (6.24 wt.%), and a natural sodalite for Cl (6.82 wt.%). Natural albite, bytownite, and orthoclase were used as standards for the feldspar analyses. Count data were stored, and analyses computed online, using the data-reduction scheme FRAME (Yakowitz et al., 1973).

Table 2. Electron-microprobe analyses and structural formulae for representative acmite and augite grains

	ACMITE								AUGITE					
	Lithic-wacke inclusions								Zeolitic clots (range of 7)	Lithic-wacke inclusions		Ultramafic		
	CYP52,II		CYP52,IV		CYP8,II		CYP8,B			CYP101, VII	CYP8, D	host		
	Core	Rim	Core	Rim	Core	Rim	Core	Rim				(range of 28)		
SiO ₂	52.9	52.5	53.0	54.4	53.2	53.9	53.2	52.9	51.6 - 53.2	52.8	53.1	51.3 - 55.9		
TiO ₂	8.38	1.24	10.0	6.91	5.83	0.12	7.21	0.72	1.64 - 4.41	0.68	0.85	0.19 - 1.41		
Al ₂ O ₃	0.32	0.39	0.31	0.28	0.34	0.71	0.18	0.47	0.22 - 1.27	0.42	0.68	0.18 - 1.57		
Fe ^T	21.8	26.9	19.9	22.1	22.8	28.3	22.8	29.3	24.0 - 31.7	11.7	10.7	3.80 - 10.11		
Fe ₂ O ₃ ^C	15.66	29.93	13.22	19.48	22.79	31.45	19.16	31.81	20.9 - 34.9	1.92	2.32	0.17 - 4.82		
Fe ^C	7.68	—	8.03	4.60	2.24	—	5.54	0.65	0.27 - 5.23	9.96	8.61	1.74 - 8.36		
MnO	0.05	0.05	0.05	0.09	0.01	0.01	0.05	0.02	0.16 - 0.22	0.42	0.31	0.08 - 0.46		
MgO	1.78	1.24	1.97	2.09	2.34	1.66	1.74	1.01	0.00 - 2.40	12.7	12.0	11.9 - 15.9		
CaO	1.11	0.93	0.98	0.62	1.03	0.93	0.21	0.11	0.14 - 3.86	19.3	20.6	21.2 - 25.4		
Na ₂ O	12.6	13.0	12.8	13.1	13.2	13.2	13.1	13.2	11.3 - 13.4	1.28	1.65	0.51 - 2.15		
K ₂ O	—	—	—	—	—	0.02	—	—	—	—	—	—		
Total*	100.44	99.32	100.36	101.57	100.98	102.00	100.39	100.79	—	99.48	99.82	—		
Si	1.994	2.008	1.991	2.014	1.985	2.008	2.002	2.001	—	—	1.991	1.988	—	
Al	0.006	—	0.009	—	0.015	—	—	—	—	—	0.009	0.012	—	
Tet.	2.000	2.008	2.000	2.014	2.000	2.008	2.002	2.001	—	—	2.000	2.000	—	
Al	0.009	0.018	0.005	0.012	—	0.031	0.008	0.021	—	—	0.010	0.018	—	
Fe ³⁺	0.444	0.862	0.374	0.543	0.642	0.882	0.543	0.906	—	—	0.055	0.065	—	
Fe ²⁺	0.242	—	0.252	0.143	0.070	—	0.174	0.020	—	—	0.314	0.270	—	
Mg	0.100	0.071	0.110	0.115	0.130	0.092	0.098	0.057	—	—	0.715	0.667	—	
Mn	0.002	0.002	0.002	0.003	—	—	0.002	0.001	—	—	0.013	0.010	—	
Ti	0.237	0.036	0.283	0.192	0.164	0.003	0.204	0.020	—	—	0.019	0.024	—	
M(1)	1.033	0.989	1.026	1.008	1.006	1.008	1.029	1.025	—	—	1.126	1.054	—	
X _{oct}	0.033	—	0.026	0.008	0.006	0.008	0.029	0.025	—	—	0.126	0.054	—	
Ca	0.045	0.040	0.039	0.025	0.041	0.037	0.008	0.004	—	—	0.780	0.826	—	
Na	0.922	0.962	0.935	0.940	0.954	0.956	0.959	0.968	—	—	0.094	0.120	—	
M(2)	1.000	1.002	1.000	0.973	1.001	1.001	0.996	0.998	—	—	1.000	1.000	—	
Fe/(Fe+Mg)	0.873	0.924	0.850	0.856	0.845	0.906	0.880	0.942	—	—	0.340	0.334	—	
NaFe ³⁺ Si ₂ O ₆	0.444	0.871	0.374	0.552	0.642	0.898	0.544	0.904	—	—	0.055	0.065	—	
NaAlSi ₂ O ₆	0.009	0.018	0.005	0.012	—	0.031	0.008	0.021	—	—	0.010	0.018	—	
NaMg _{0.5} Ti _{0.5} Si ₂ O ₆	0.200	0.073	0.220	0.233	0.260	0.006	0.196	0.040	—	—	0.029	0.037	—	
NaFe _{0.5} Ti _{0.5} Si ₂ O ₆	0.269	—	0.336	0.156	0.052	—	0.213	—	—	—	—	—	—	
CaTiAl ₂ O ₆	0.003	—	0.005	—	0.007	—	—	—	—	—	0.005	0.006	—	
CaMnSi ₂ O ₆	0.002	0.002	0.002	0.003	—	—	0.002	0.001	—	—	0.013	0.010	—	
Ca ₂ Si ₂ O ₆	0.020	0.019	0.016	0.011	0.017	0.019	0.003	0.002	—	—	0.382	0.405	—	
Mg ₂ Si ₂ O ₆	—	0.017	—	—	—	0.046	—	0.029	—	—	0.349	0.324	—	
Fe ₂ Si ₂ O ₆	0.053	—	0.042	0.033	0.022	—	0.034	0.003	—	—	0.157	0.135	—	

*Includes Fe₂O₃^C and Fe^C.

Fe^T corresponds to microprobe determination of total Fe.

Fe₂O₃^C and Fe^C are values generated by the computer program of Papike *et al.* (1974).

Pyroxenes

The 10 selected pyroxene analyses listed in Table 2 represent a total of 22 acmite and 7 augite analyses from four samples. High sums for two of the acmite analyses apparently relate to difficulty in reoccupying portions of these strongly, and nonuniformly, zoned crystals. Distribution of

Fe³⁺/Fe²⁺ and structural formulae were calculated with the computer program of Papike *et al.* (1974). Normative pyroxene components were calculated according to a procedure proposed by Malcolm Ross, U.S. Geological Survey (written communication, 1982). Relative to the cores, rims of acmite grains are enriched in Fe and depleted in Ti; the rims also generally contain slightly more Al and less Ca

and Mg. $Fe/(Fe + Mg)$ ranges from 0.830 to 0.978, and $Na/(Na + Ca)$ from 0.953 to 0.995; both ratios are always greater in the rims of grains. In agreement with Ferguson (1977), our data do not support Flower's (1974) proposal that Al, Fe, and Ti substitute significantly for tetrahedral Si in titanian acmite.

Total measured ranges (in weight percent) in the composition of acmite within lithic-wacke inclusions are: SiO_2 , 51.8–54.5; TiO_2 , 0.12–10.2; Al_2O_3 , 0.18–1.32; FeO^T , 18.5–29.3; MnO , 0.00–0.20; MgO , 0.36–2.53; CaO , 0.11–1.36; and Na_2O , 12.6–13.3. As listed in Table 2, this compositional range resembles that shown by acmite crystals that are associated with natrolite, sodalite, and pectolite in zeolite-rich clots (several cm across) within the contaminated ultramafic host. A notable exception is TiO_2 : Ti contents in the cores of some acmite grains within lithic-wacke inclusions may establish a new maximum (0.297 cation/6 oxygen ions; analysis not reported in Table 2) for pyroxenes (Robinson, 1980). Acmite in both environments may closely approach the ideal composition, $NaFe^{3+}Si_2O_6$; SiO_2 –52.02, Fe_2O_3 –34.56, Na_2O –13.42 (weight percent).

Also listed in Table 2 are compositions of the augite that typically forms a rind at the contact of inclusions with the ultramafic host but may also occur as discrete grains (maximum 8 mm) within inclusions. For comparison, we show the compositional range of the augite that is an essential constituent of the ultramafic host. There are significant differences between the two augites in the contents of Ca, Fe, and Mg. While it was expected that the augite in the ultramafic host would contain more Ca and Mg, it is surprising to find that it contains less Fe.

Figure 3 illustrates the strong compositional zoning between the Ti-rich dark-green cores and the Ti-poor Fe-enriched colorless rims: Ti content is plotted against total Fe content and $Fe^{2+}/(Fe^{2+} + Fe^{3+})$ for all acceptable analyses. Figure 3A shows a good inverse correlation, averaging 1:1, between Ti and total Fe contents; Figure 3B shows that this exchange is well accounted for by variations in $Fe^{2+}/(Fe^{2+} + Fe^{3+})$ within the crystals. Exchange of $Ti^{4+} + Fe^{2+}$ within the cores for Fe^{3+} within the rims may be regarded as substitution within the solid-solution series $NaFe^{3+}Si_2O_6$ – $Na(Fe^{2+}, Mg)_{0.5}Ti_{0.5}^{4+}Si_2O_6$ (Ferguson, 1977; Deer et al., 1978, v. 2A, p. 486, 493). The reference lines in Figure 3 are for a specific case in which one-third of a total of 0.9 Fe cations was initially Fe^{2+} , coupled with Ti^{4+} . Poor correlation of Ti content with $Fe/(Fe + Mg)$, indicates that Mg is not fundamentally involved in the coupling and substitution mechanism (note the moderate and relatively uniform MgO content of these acmites).

Relations between Na and Ti in pyroxenes are complex as is evident from the data of Flower (1974, Fig. 6) and Ronsbo et al. (1977, Fig. 2). At Coyote Peak, marked depletion of Ti from core to rim of acmite grains is typically accompanied by only slight enrichment in Na (Table 2); this is in agreement with Ferguson (1977, p. 250), who noted that minor Ca may substitute for Na with increasing Ti content, although the zoning pattern he referred to is the

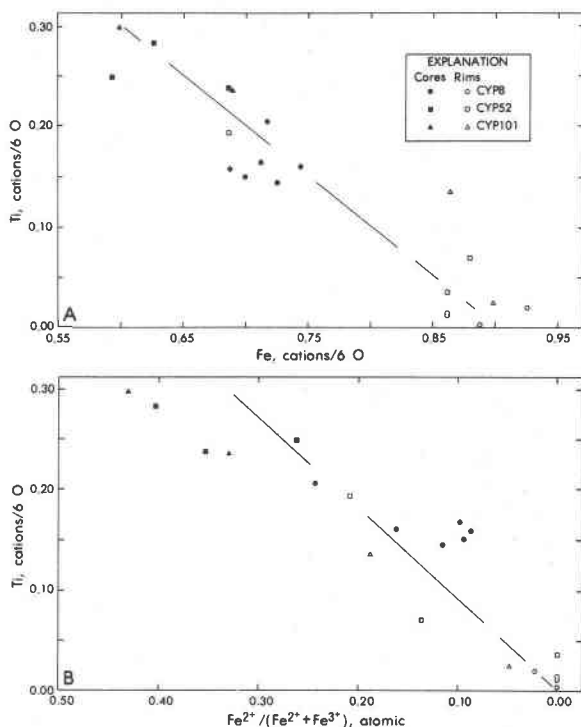


Fig. 3. (A) Relation between Ti and total Fe contents in zoned pyroxenes. (B) Relation between Ti content and atomic $Fe^{2+}/(Fe^{2+} + Fe^{3+})$ in zoned pyroxenes.

reverse of that observed in Coyote Peak acmite. Continuing loss of Ab component from adjacent feldspars may explain the continued availability of Na at the time of rim crystallization.

Although the number of analyses is not great, we note that pyroxene cores in sample CYP8, the small homogeneous inclusion, are lower in Ti^{4+} and Fe^{2+} contents than the pyroxene cores in sample CYP52, a medium-size zoned inclusion. As discussed below, amphibole chemistry shows even sharper, size-dependent variation.

Because titanian acmites have recently received much attention (e.g., Ferguson, 1977; Ronsbo et al., 1977; Nielsen, 1979), it seems appropriate to reflect briefly on nomenclature and calculation schemes for these pyroxenes. In addition to the calculations listed in Table 2, we have recalculated the 7 analyses in Table 1 of Ferguson (1977), the 7 analyses in Table 2 of Ronsbo et al. (1977), and the 10 analyses in Table 4 of Nielsen (1979). We have used the end-member components and the order of calculation (Table 2) proposed by Malcolm Ross (written communication, 1982). Of 34 analyses, only 21 calculate out to give residuals (i.e., cations which cannot be allocated to an end member) of less than 0.020 cation, and these give an average residual of 0.004 cation; larger residuals for other analyses suggest that those analyses are inferior. For example, analyses of three rims of grains from Coyote Peak calculate out with residuals (in cations) as follows: CYP52, IIR—Na, 0.010 and Si, 0.027; CYP52, IVR—Si,

0.042; and CYP8,II,R—Na, 0.037 and Si, 0.044. Because the cores of these grains give an average residual of 0.001 cation, we suspect that crystal heterogeneity and uncertainty in beam relocation caused the residuals for the rims. For analysis 7 of Ronsbo et al. (1977) and analysis 6 of Nielsen (1979), residuals of 0.043 and 0.023 cation were reduced to 0.002 and 0.001 cation, respectively, by insertion of the component NaTiAlSiO_6 in lieu of $\text{CaTiAl}_2\text{O}_6$; for analyses 7 and 8 of Nielsen, large residuals were cut in half by use of this component. However, unacceptable residuals of 0.048 to 0.251 cation remain for the latter two analyses, for analysis 4 of Ronsbo et al., for analyses 1, 4, 5, and 6 of Ferguson, for analyses 2 and 3 in Table 5 of Ronsbo et al., and for analysis 19 in Table 53 of Deer et al. (1978, p. 492). Therefore, we believe that many reported analyses of titanian acmite are in error and that care must be exercised in their acceptance. The component NaTiAlSiO_6 seems to be of questionable significance in these pyroxenes.

Figure 4 is a plot of normative components for the pyroxene compositions listed in Table 2 and the apparently superior analyses of Ferguson (1977), Ronsbo et al. (1977), and Nielsen (1979) on a modified pyroxene ternary diagram in which the end member $\text{Na}(\text{Fe}^{2+}, \text{Mg})_{0.5}\text{Ti}_{0.5}\text{Si}_2\text{O}_6$ is placed at the apex. Analysis 1 of Ferguson is also plotted, despite identical large residuals of 0.024 cation for Fe^{2+} and Ti, because it is the most Ti-rich acmite heretofore reported. Coyote Peak acmite is apparently unique in following an extended trend of low and nearly uniform mole fraction of "Quad"-plus-"Other" components.

It is significant that for the first time a composition has been determined for a pyroxene which contains more than 50 mole% of the end member $\text{Na}(\text{Fe}^{2+}, \text{Mg})_{0.5}\text{Ti}_{0.5}\text{Si}_2\text{O}_6$. Although we do not undertake here the task of naming this end member, we note the following five points: (1) It seems most unfortunate that the term "neptunite" was championed for this end member by Ferguson and taken up by Deer et al. (1978, p. 486, 493). Neptunite is not a pyroxene, and we strongly discourage use of this name. (2) In our opinion, the substitution of Ti^{4+} is of fundamental significance in setting this end member apart from acmite. Thus, we do not favor establishing two end members, namely, $\text{NaFe}_{0.5}^{2+}\text{Ti}_{0.5}\text{Si}_2\text{O}_6$ and $\text{NaMg}_{0.5}\text{Ti}_{0.5}\text{Si}_2\text{O}_6$. (3) Moreover, because the mole fractions of these two components, commonly referred to as Fe^{2+} -NAT and Mg -NAT (e.g., Cameron and Papike, 1981), generally depend significantly on the order of calculation and thus can be misleading, we recommend that discussion in these terms be abandoned. (4) Failing that, and in consideration of our data summarized in Figure 3, we suggest that there is good cause to reverse the common order of calculation for these pyroxene components containing M(1)-M(2) cations of four valencies (Na^+ , Fe^{2+} , Fe^{3+} and Ti^{4+}), such that the component $\text{NaFe}_{0.5}^{2+}\text{Ti}_{0.5}\text{Si}_2\text{O}_6$ is calculated before the component $\text{NaMg}_{0.5}\text{Ti}_{0.5}\text{Si}_2\text{O}_6$. (5) Following common usage, these pyroxenes might best be called simply "titanian acmite" until the end member is established as a new mineral species.

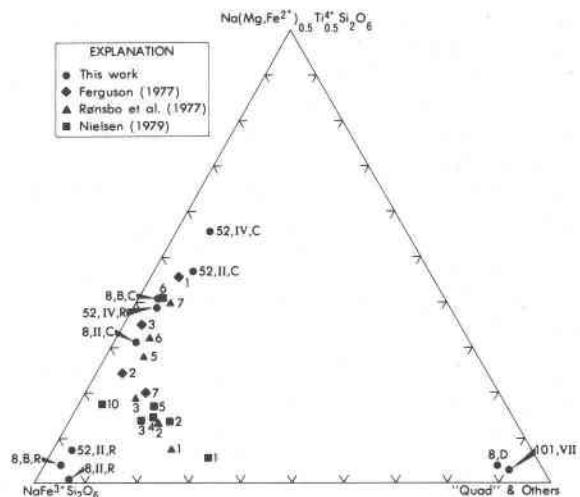


Fig. 4. An improvised pyroxene ternary diagram in which the components $\text{Na}(\text{Fe}^{2+}, \text{Mg})_{0.5}\text{Ti}_{0.5}\text{Si}_2\text{O}_6$ and $\text{NaFe}^{3+}\text{Si}_2\text{O}_6$ have been isolated and all other components (see Table 2) have been combined with the "Quad" components at a third corner. Sample designations are the same as in Table 2, and for the other references are from respective tables cited in text.

Amphiboles

A total of 47 amphibole analyses were obtained, representing 29 grains in samples CYP7, CYP8, CYP52, CYP101, and CYP178. In most cases, core and rim compositions were determined for these conspicuously, but non-uniformly, zoned grains (see Figs 2D and 2E). Table 3 lists data for representative analyses, and data for all analyses from samples CYP8, CYP52, and CYP101 are included in a series of plots (Figs. 5, 6, and 7) to depict the substitution relations found in these alkali amphiboles. Table 3 also lists structural formulae, and "midpoint" values of Fe_2O_3 and FeO calculated with the amphibole calculation program of Papike et al. (1974). Because of the heterogeneity, small size, and intergrowth of these amphibole grains, we have not pursued their optical and X-ray properties.

Typically, the amphibole cores are ferroan richterite, and the rims titanian magnesio-arfvedsonite (Leake, 1978; Hawthorne, 1981). Low Al content leads to a designation as arfvedsonite rather than eckermannite. Considering their uniformly low Al_2O_3 contents, and CaO contents that may fall below 1 weight percent, the arfvedsonitic rims appear to be among the nearest to ideal composition yet reported, with one caveat—they contain Ti^{4+} rather than Fe^{3+} . (In fact, we use the term "arfvedsonite" with misgiving and believe that eventually the designation of a titanian alkali-amphibole end member, $\text{NaNa}_2(\text{Fe}, \text{Mg})_{4.5}\text{Ti}_{0.5}\text{Si}_8\text{O}_{22}(\text{OH})_2$, may be justified.) Their zoning thus provides a fascinating contrast to the pyroxene zoning. Most analyses represent compositions that should properly be prefixed "ferroan," "fluor-," and (or) "titanian"; for simplicity, we sometimes refer to these amphiboles as richterites.

Most of our analyses contain insufficient Si and Al to fill

Table 3. Electron-microprobe analyses and structural formulae for representative amphibole grains in lithic-wacke inclusions and zeolitic clots

	CYP8,II		CYP8,V		CYP52,V		CYP52,IX		CYP101,II		CYP101,V		Zeolitic clots (range of 5)
	Core	Rim	Core	Rim	Core	Rim	Core	Rim	Core	Rim	Core	Rim	
SiO ₂	55.8	54.6	55.5	54.3	55.0	54.1	55.5	54.5	55.1	53.0	56.0	52.9	51.3 - 54.8
TiO ₂	2.19	2.95	2.21	3.59	2.46	3.49	3.13	4.87	1.54	6.21	2.02	6.39	1.47 - 2.97
Al ₂ O ₃	0.38	0.24	0.29	0.19	0.29	0.11	0.30	0.24	0.37	0.25	0.40	0.19	0.62 - 1.41
FeO ^I	7.76	13.8	9.93	20.1	8.47	11.22	9.58	17.5	7.89	17.9	9.34	23.8	15.7 - 19.5
Fe ₂ O ₃ ^C	—	0.87	0.56	1.39	—	—	—	—	—	—	—	—	—
FeO ^C	7.76	12.99	9.43	18.81	8.47	11.22	9.58	17.5	7.89	17.9	9.34	23.8	—
MnO	0.04	0.12	0.11	0.13	0.06	0.06	0.09	0.09	0.14	0.25	0.20	0.23	0.37 - 0.66
MgO	17.8	13.9	17.1	8.93	17.6	15.3	16.7	10.3	19.0	9.44	17.8	4.73	9.48 - 10.8
CaO	4.61	1.60	3.19	0.49	5.64	4.67	5.15	2.26	6.19	4.52	5.99	2.66	0.05 - 3.53
Na ₂ O	6.52	8.19	7.22	8.82	6.17	6.61	6.42	7.79	6.08	6.52	6.17	6.93	6.17 - 7.70
K ₂ O	1.67	1.72	1.58	1.71	1.63	1.60	1.60	1.58	1.43	1.55	1.36	1.52	3.36 - 4.76
F*	2.60	1.31	1.94	0.88	2.96	2.01	2.20	1.13	3.66	1.24	3.41	1.01	0.74 - 1.48
Total**	98.28	97.94	98.31	98.97	99.03	98.32	99.74	99.78	99.36	100.36	101.25	99.93	
Si	7.979	7.975	7.961	8.047	7.872	7.860	7.879	7.946	7.843	7.755	7.874	7.928	—
Al	0.021	0.025	0.039	—	0.049	0.019	0.050	0.041	0.062	0.043	0.066	0.034	—
Ti	—	—	—	—	0.079	0.121	0.071	0.013	0.095	0.202	0.060	0.038	—
Tet.	8.000	8.000	8.000	8.047	8.000	8.000	8.000	8.000	8.000	8.000	8.000	8.000	—
Al	0.043	0.016	0.010	0.033	—	—	—	—	—	—	—	—	—
Fe ³⁺	—	0.095	0.060	0.155	—	—	—	—	—	—	—	—	—
Fe ²⁺	0.927	1.587	1.132	2.330	1.014	1.364	1.138	2.139	0.939	2.191	1.099	2.989	—
Mg	3.782	3.025	3.650	1.971	3.763	3.310	3.536	2.226	4.023	2.059	3.735	1.056	—
Mn	0.005	0.015	0.013	0.016	0.007	0.007	0.011	0.011	0.017	0.031	0.024	0.029	—
Ti	0.235	0.324	0.239	0.400	0.186	0.261	0.264	0.521	0.070	0.481	0.154	0.682	—
M(1)-M(3)	4.992	5.062	5.104	4.905	4.970	4.942	4.949	4.897	5.049	4.762	5.012	4.756	—
X _{oct}	—	0.062	0.014	—	—	—	—	—	0.049	—	0.012	—	—
Ca	0.706	0.251	0.491	0.078	0.865	0.727	0.784	0.353	0.944	0.709	0.903	0.427	—
Na	1.294	1.687	1.405	1.922	1.135	1.273	1.216	1.647	1.007	1.291	1.085	1.573	—
M(4)	2.000	2.000	2.000	2.000	2.000	2.000	2.000	2.000	2.000	2.000	2.000	2.000	—
Na	0.512	0.632	0.606	0.611	0.576	0.591	0.553	0.555	0.670	0.559	0.598	0.441	—
K	0.304	0.321	0.289	0.323	0.298	0.297	0.290	0.294	0.260	0.289	0.244	0.291	—
A	0.816	0.953	0.895	0.934	0.874	0.888	0.843	0.849	0.930	0.848	0.842	0.732	—
Na/(Na+K)	0.856	0.878	0.874	0.887	0.852	0.863	0.859	0.882	0.866	0.865	0.873	0.874	—
Fe/(Fe+Mg)	0.197	0.357	0.246	0.558	0.212	0.292	0.243	0.490	0.189	0.516	0.227	0.739	—
RIC-MAX	0.706	0.251	0.491	0.078	0.865	0.727	0.784	0.353	0.930	0.709	0.842	0.427	—
ARF-MAX	0.470	0.648	0.478	0.795	0.372	0.522	0.528	0.824	0.140	0.646	0.308	0.732	—

*No Cl is present.

**Based on calculated Fe₂O₃ and FeO values and corrected for 0 equivalent to F.

the tetrahedral sites (see Table 3). On the basis of extensive experience with our analytical procedure, we consider this deficiency to be real and have filled the tetrahedral sites with Ti (Papike et al., 1969; Charles, 1977). The deficiency in tetrahedral Si in these amphiboles is compatible with Ernst's (1962) discovery that arfvedsonitic amphiboles are

silica deficient if formed at oxygen fugacities lower than those defined by the hematite-magnetite buffer. Ernst suggested that Fe³⁺ may replace tetrahedral Si in arfvedsonitic amphiboles formed at low oxidation states. Charge and similar effective radius (Whittaker and Muntus, 1970) make Ti⁴⁺ an equally or more acceptable replacement for Si⁴⁺

in these amphiboles, in which Fe^{3+} is an insignificant component.

Comparison with the compositions of amphiboles found within zeolitic clots in the contaminated ultramafic host shows that amphiboles in the lithic-wacke inclusions have higher Ti and lower Al contents, a result opposite to what might have been expected, based on the whole-rock compositions of samples CYP4 and CYP5. The amphiboles within the zeolitic clots also are notably richer in K and Mn and do not range so widely in Mg content; none contain so much Mg as do the cores of grains within the inclusions.

Charles (1975, 1977) studied the phase equilibria of end-member and intermediate compositions in the system $\text{Na}_2\text{CaMg}_5\text{Si}_8\text{O}_{22}(\text{OH})_2\text{--Na}_2\text{CaFe}_3\text{Si}_8\text{O}_{22}(\text{OH})_2$ under varying f_{O_2} - T conditions and concluded that the richterite-ferro-richterite series represents a complete solid solution between end members. This conclusion is consistent with a plot of Fe^{VI} versus Mg^{VI} in the amphiboles from Coyote Peak (Fig. 5), in which there is a nearly continuous substitution of Fe for Mg over the rather extensive range of analyzed complex amphiboles.

Papike et al. (1969) indicated that two alkali ions couple with a single Ca^{2+} ion in the richterite lattice, such that an equal number of Na and Ca cations occupy the M(4) site and Na occupies the A site. A plot of $\text{Na}^{\text{M(4)}}$ versus Ca content (Fig. 6) supports the idea of Na substitution for Ca: richterite cores are relatively enriched in Ca and approach $\text{Na}:\text{Ca} = 1:1$ in the M(4) site, whereas corresponding arfvedsonitic rims are enriched in Na relative to Ca and approach $\text{Na}:\text{Ca} = 2:0$ in the M(4) site. We cannot entirely explain the deviations from ideal Na-for-Ca substitution reflected in Figure 6. In most cases, however, the de-

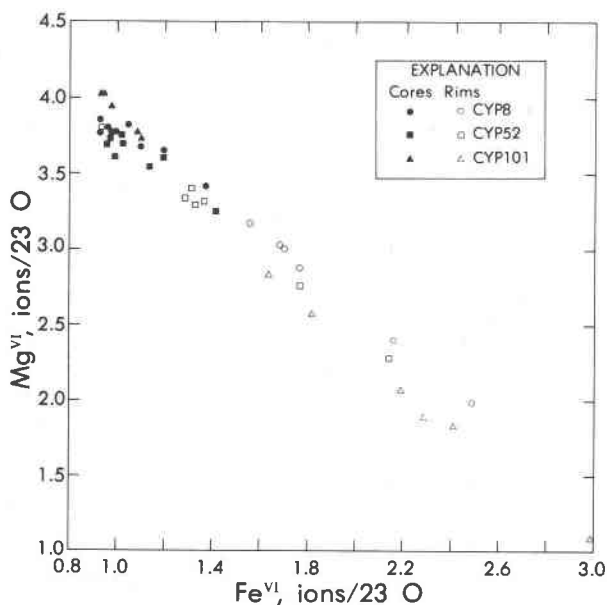


Fig. 5. Relation between Mg and Fe occupancy of octahedral sites in zoned alkali amphiboles.

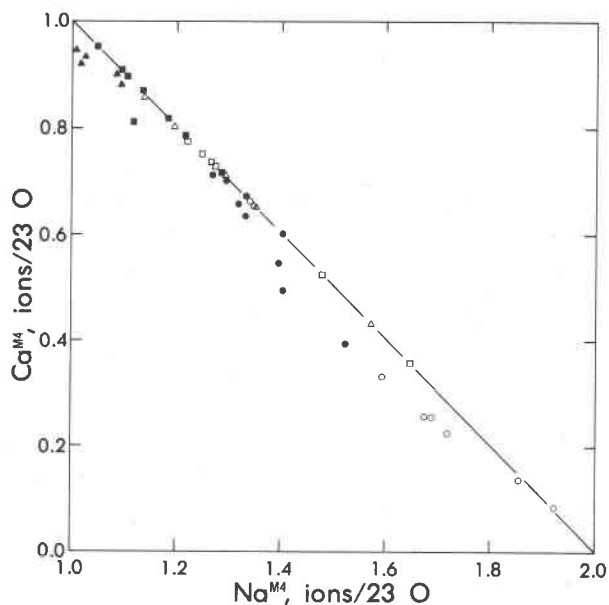
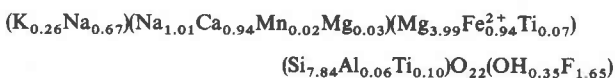


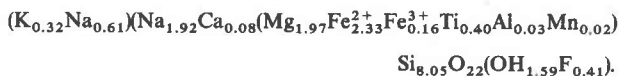
Fig. 6. Relation between Ca and Na occupancy of M(4) site in zoned alkali amphiboles.

viant points correlate with calculated octahedral-site occupancies of over 5 cations and thus may be an artifact of the calculation scheme.

Because the classification of alkali amphiboles does not yet depend on TiO_2 content, the extreme compositions may be regarded as those listed in Table 3 for the core of grain CYP101,II and the rim of grain CYP8,V. Corresponding formulae, showing the shift in Na and Ca occupancy of the M(4) site, are:



and



Clearly reflected in these two formulae is the relative constancy of A-site occupancy, in contrast to the substantial differences in constitution of the M(4) and M(1)–M(3) sites. The work of Huebner and Papike (1970) suggests complete solid solution between K and Na in the A site of the richterite lattice. Consideration of Table 3 shows that the K content of the A site varies little (0.22–0.32 cation for the full data set) and that A-site Na content may increase or decrease from core to rim for individual grains.

Ti is a significant element in amphibole substitution mechanisms, as shown by many recent microprobe analyses of arfvedsonitic amphiboles occurring with titanian acmite in peralkaline and undersaturated rocks (e.g., Scott, 1976; Ronsbo et al., 1977; Grapes et al., 1979; Nielsen, 1979). However, none of these analyses approaches the

Coyote Peak rim compositions with respect to Ti^{4+} content, which may reach 0.7 cation per formula unit; Ti appears partly to fill the tetrahedral site and totally supplants Fe^{3+} in the M(1)–M(3) sites. Figures 7A and 7B show good correlations between Ti^{VI} content (cations/23 oxygen ions) and both $Fe/(Fe + Mg)$ and $Na/(Na + Ca)$. Whereas the data of Table 3 can be taken to suggest that total Ti, Fe, and Na contents are related, poorer correlations than those of Figures 7A and 7B result when Ti^{IV+VI} content is plotted versus $Fe/(Fe + Mg)$ and $Na/(Na + Ca)$, indicating that Ti^{VI} is the more significant variable (as well as supporting assignment of Ti^{4+} to the tetrahedral site). We note that because Fe^{3+} is not a significant component in these amphiboles, the charge-balancing mechanism is apparently $Ti^{4+} + Na^+$ for $Mg^{2+} + Ca^{2+}$ and should not be intrinsically sensitive to oxygen fugacity. The Ti-rich Coyote Peak amphiboles are of special interest in view of considerable discussion over the mechanisms of incorporation of Fe^{3+} and Ti^{4+} into the amphibole structure (e.g., Whittaker, 1949 and 1960; Ghose, 1966; Charles, 1974; Kitamura et al., 1975). Table 3 reveals poor correlation among: (1) occupancy of Ti^{4+} in the M(1)–M(3) sites, (2) Na in the M(4) site, and (3) A-site occupancy. Our data do not support the inverse relations based on charge balancing that have been proposed for accommodation of Fe^{3+} and Ti^{4+} .

Calculation of amphibole norms in the manner presented for the pyroxenes requires too many assumptions regarding end members and priorities of calculation. However, for comparative purposes only, we have calculated independently the maximum mole fraction of each of the two end members $(Na,K)CaNa(Fe,Mg)_5Si_8O_{22}(OH)_2$ and $(Na,K)Na_2(Fe,Mg)_{4.5}Ti_{0.5}Si_8O_{22}(OH)_2$ which can be derived from the structural formulae listed in Table 3; these values are listed at the foot of Table 3 as RIC-MAX and ARF-MAX. A notable result of attempts to calculate amphibole end members was the realization that the rims of grains CYP52,IX, CYP101,II, and CYP101,V contain substantially more Ti than can be accommodated by the proposed titanian-arfvedsonite end member. Moreover, Table 3 shows that the calculated occupancy of M(1)–M(3) sites is significantly less than 5 for the Ti-enriched compositions. The existence of such electrochemically balanced, but cation-deficient components as $(Na,K)Na_2Fe_3TiSi_8O_{22}(OH)_2$ and $[]CaNa_2Fe_3TiSi_8O_{22}(OH)_2$ must also be considered.

Strikingly apparent in Figure 7B are the distinct chemical-evolution paths that characterize amphiboles from individual inclusions and that apparently are a function of inclusion size. These trends are even better defined in Figure 7C, in which $Fe/(Fe + Mg)$ is plotted against $Na/(Na + Ca)$. Both Figures 7B and 7C show that amphibole cores within the three inclusions are relatively similar in composition but evolve to strikingly different rim compositions.

Fluorine, an element that has a large affect on amphibole stability, varies significantly in concentration from core to rim within the amphiboles and with respect to $Fe/(Fe + Mg)$ (Fig. 7D). The O3 site in amphiboles is coordi-

nated by one M(3) and two M(1) cations. Cameron and Gibbs (1973) showed that entry of F into this site reduces the size of the M(1) and M(3) sites and of the octahedral layer as a whole. Rosenberg and Foit (1977) showed that Fe^{2+} is not favored in F-coordinated sites due to smaller crystal field-stabilization energy. Thus, the more F- and Mg-rich amphibole cores can represent a more thermally stable phase characterized by relatively strong Mg–F bonds and restriction of Fe^{2+} to the M(2) site. The amphiboles evolve toward compositions of lower thermal stability containing less F and more Fe (Fig. 7D). A plot of F content versus $Na/(Na + Ca)$ (Fig. 7E) supports data presented elsewhere which show that richterite cores, enriched in F + Ca, also evolve into rims enriched in Na and low in F. Figures 7D and 7E reveal that F content in the growing amphiboles also appears to have been a function of inclusion size. As for the pyroxenes, amphibole cores in the smallest inclusion (sample CYP8) are more “evolved” than those in the larger inclusions; they contain less F (Figs. 7D and 7E) and have a higher $Na/(Na + Ca)$ (Figs. 7B, 7C, and 7E).

The zeolite-rich clots within the contaminated ultramafic host are thought to have crystallized from a late-stage fluid-rich phase. The similar compositions of amphiboles and pyroxenes within these clots and the lithic-wacke inclusions result not from any relation between the two features, but from a common environment imposed by the ultramafic host.

Feldspars

The analyses listed in Table 4 represent 34 analyses of feldspars within lithic-wacke inclusions and a sample of the intruded Franciscan assemblage (CYP4) taken a few meters from the intrusive diatreme contact. Recall that the ultramafic host is nepheline bearing, and contains no feldspar.

Sample CYP4 contains relic plagioclase grains of near-ideal albitic composition ($Ab_{99.6}Or_{0.2}An_{0.2}$) that are quite homogeneous, considering that the analyses include core and rim compositions for six grains. This plagioclase is unusually sodic for Franciscan graywacke (Bailey et al., 1964), and it is possible that intrusion of the diatreme albited this plagioclase without affecting rock textures.

As discussed earlier, it seems difficult to prove that the lithic-wacke inclusions were identical to the lithic-wacke wallrock at the present level of exposure. We perhaps make that assumption most explicitly in the following discussion, in which we interpret our analyses to establish a progressive, but commonly aborted, exchange reaction whereby K was exchanged for Na within relic feldspar grains. Feldspar grains in the cores or at the core-rim interface of larger inclusions have a different range of compositions from those found in more uniformly altered small inclusions or near the margins of larger inclusions. Plagioclase in the core assemblage typically is strongly zoned, with K/Na higher in the rims of grains (Table 4). The examples chosen for Table 4 represent extremes of K_2O content; in the core assemblage, no grains approaching pure albite have been found, and compositions near pure $KAlSi_3O_8$ are not

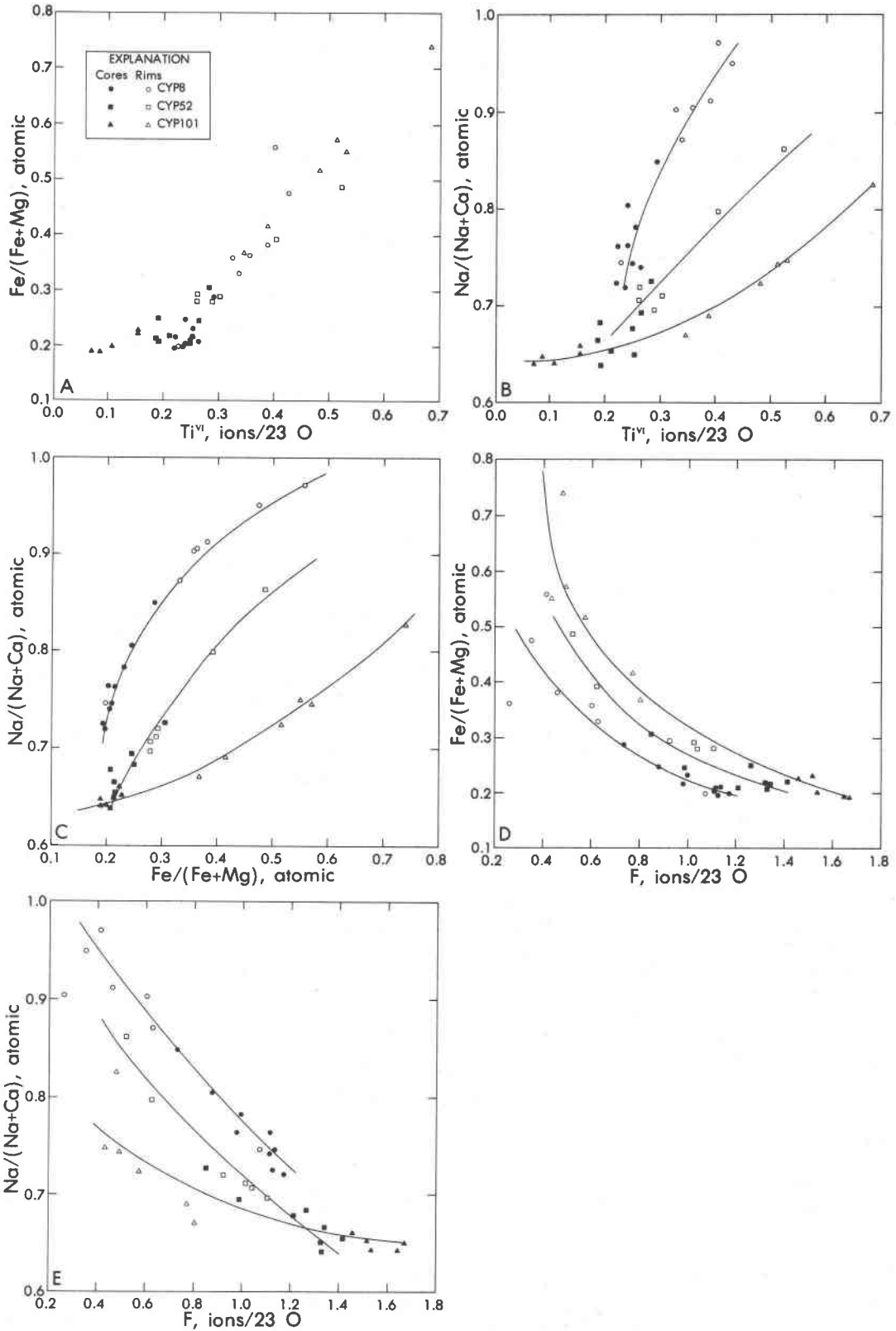


Fig. 7. Compositional relations for zoned alkali amphiboles. Curves qualitatively illustrate relations within inclusions of three sizes. (A) $\text{Fe}/(\text{Fe} + \text{Mg})$ versus Ti^{VI} content. (B) $\text{Na}/(\text{Na} + \text{Ca})$ versus Ti^{VI} content. (C) $\text{Na}/(\text{Na} + \text{Ca})$ versus $\text{Fe}/(\text{Fe} + \text{Mg})$. (D) $\text{Fe}/(\text{Fe} + \text{Mg})$ versus F content. (E) $\text{Na}/(\text{Na} + \text{Ca})$ versus F content.

Table 4. Electron-microprobe analyses and structural formulae (based on 32 oxygen ions) of feldspar grains within lithic-wacke country rock and inclusions

	Lithic-wacke country rock			Cores of larger lithic-wacke inclusions				Rims and small inclusions		
	CYP4		Core	Rim	CYP7,D2		CYP52,G2	CYP8,C		
	Average*	Range*			Core	Rim		Dusty Core	Clear Rim	
SiO ₂	69.15	67.6 - 70.7	66.2	66.7	68.3	66.0	65.7	65.5	64.9	
Al ₂ O ₃	19.74	19.0 - 20.4	20.9	19.8	19.5	19.5	19.0	19.1	19.3	
CaO	0.04	0.00 - 0.09	0.80	0.33	0.14	0.15	0.09	0.07	0.02	
Na ₂ O	11.67	11.4 - 11.8	8.28	6.37	9.47	2.14	0.17	0.32	0.08	
K ₂ O	0.05	0.02 - 0.08	4.24	7.59	3.28	13.81	16.28	15.83	16.36	
Total	100.65		100.42	100.79	100.69	101.50	101.24	100.82	100.66	
Si	11.990	-- --	11.708	11.868	11.972	11.892	11.968	11.960	11.908	
Al	4.040	-- --	4.356	4.160	4.036	4.148	4.080	4.112	4.164	
Sum	16.030		16.064	16.028	16.008	16.040	16.048	16.072	16.072	
Ca	0.010	-- --	0.152	0.064	0.024	0.028	0.020	0.012	0.004	
Na	3.920	-- --	2.840	2.196	3.220	0.748	0.060	0.116	0.028	
K	0.010	-- --	0.956	1.724	0.732	3.176	3.784	3.684	3.828	
Sum	3.940		3.948	3.984	3.976	3.952	3.864	3.812	3.860	
An	0.2	-- --	3.9	1.6	0.6	0.7	0.5	0.4	0.1	
Ab	99.6	-- --	71.9	55.1	81.0	18.9	1.6	3.0	0.7	
Or	0.2	-- --	24.2	43.3	18.4	80.4	97.9	96.6	99.2	

*For 14 analyses of 8 grains.

reached. Quartz and lithic fragments make up about 60% of sample CYP4 and typically 55 to 90% of Franciscan graywacke (Bailey et al., 1964), yet are rare in the inclusion cores; it appears, therefore, that a significant proportion of the intermediate alkali feldspar in these cores has been created by feldspathization of these constituents. In contrast to the cores, the predominant feldspar in more uniformly metasomatized small inclusions is nearly end-member $KAlSi_3O_8(Or_{96.6-99.2}Ab_{0.7-3.0}An_{0.1-0.3})$. Such grains may be "dusty" or clear, or may display a dusty core and clear rim (Figs. 2C and 2E), showing little compositional contrast (Table 4). Within the rim assemblage of larger inclusions, feldspars show a greater range in composition (we have analyzed a grain core containing 9.4 wt.% Na₂O in the rim of sample CYP101); nearly complete exchange is typical only near the margin of the inclusion. Within the rim assemblage, feldspar grains are commonly surrounded by phases (e.g., acmite or natrolite-like zeolite) that presumably have incorporated a part of the Na released by alkali exchange.

Zeolites and related phases

Table 5 lists analyses of the natrolite-like zeolite and related phases. Its common occurrence as an interstitial phase (e.g., Figs. 2C, 2E, and 2F) suggests that the natrolite-like zeolite crystallized last. Both the natrolite-like zeolite and the fibrous, unidentified Ca-Na silicate are more conspicuous in the smaller, more nearly uniformly

recrystallized inclusions and commonly are intimately intergrown (Fig. 2F); it is difficult to ascertain whether the phases are in a reaction relation. Spatial distribution suggests that the natrolite-like zeolite, which is the dominant zeolite species toward the edges of smaller inclusions, is encroaching on the fibrous Ca-Na silicate, which is more abundant toward the centers of these inclusions. However, formation of the less common fibrous silicate may also have resulted from local chemical variations. Identification of the Na-rich zeolite as a natrolite-like mineral is based not only on the microprobe analyses but also on the X-ray powder-diffraction pattern which is similar to that of natrolite.

The X-ray powder-diffraction pattern of the fibrous, unidentified Ca-Na silicate in sample CYP52 is nearly identical to that of gonnardite (XPDF 10-473). However, the electron-microprobe analyses of this phase differ from those reported for gonnardite. Perhaps the Ca-Na silicate is a new mineral which has a crystal structure similar to that of the gonnardite but is substantially different in chemical composition; or perhaps this phase is a gonnardite that has undergone alteration and changed composition but still retains enough of the structure to give the gonnardite X-ray pattern. Further study of this phase is made difficult by its intergrown and fine-grained occurrence (Fig. 2F).

Stilpnomelane is a common phase in Franciscan wackes (Ernst, 1965) and Table 6 lists analyses of three grains of a

Table 5. Electron-microprobe analyses of natrolite-like and related phases

	Natrolite-like phase					Fibrous unidentified Ca-Na silicate			Pectolite	Wollastonite
	CYP8,A	CYP8,B	CYP178,A	CYP52,A	CYP52,B	CYP52,C	CYP52,D	CYP52,E	CYP7,C	CYP7,F
SiO ₂	39.3	39.3	41.5	43.5	43.6	47.2	46.1	44.4	52.9	51.8
Al ₂ O ₃	27.4	26.9	26.1	25.8	26.2	12.2	13.5	15.1	0.00	0.07
CaO	2.15	3.40	0.87	0.40	0.12	18.9	14.3	14.2	33.8	45.4
Na ₂ O	13.1	12.4	14.2	15.6	15.8	10.1	12.1	11.3	8.53	0.05
K ₂ O	0.03	0.02	0.06	0.10	0.04	0.06	0.21	0.05	0.07	0.00
Total	81.98	82.02	82.73	85.40	85.76	88.46	86.21	85.05	95.30	97.32*

*Also: FeO^T, 1.18; MgO, 0.25; and MnO, 0.39.

stilpnomelane-like phase from samples CYP7 and CYP101. (A typical stilpnomelane analysis is also listed for comparison.) This phase is common in other samples, although the grains are typically too small to attempt microprobe analyses.

The best X-ray powder-diffraction patterns that could be obtained show a strong broad line centered on 12.3Å and a weak broad line at 7.49Å that may belong to this phase. Other stilpnomelane lines that should have been present were not detected. An attempt to establish the identity of the stilpnomelane-like phase through use of the transmission electron microscope (TEM) was of limited success. A good 12Å repeat was seen, but the crystal showed a great deal of disorder. However, microbeam X-ray fluorescence analysis concurrent with the TEM study suggested that the high and atypical (for stilpnomelane) Ca contents indicated by some of the routine microprobe analyses may be due to intergrowth with a Ca-rich phase.

Also listed in Table 6 are analyses of several minor sheet-silicate phases in the lithic-wacke country rock and in the

core of a large inclusion (sample CYP178). None of these phases show any visible relation to stilpnomelane genesis.

Quartz

Although quartz is a major constituent of the lithic-wacke country rock at Coyote Peak, it is a minor phase in the core assemblage of large inclusions and is absent from smaller inclusions and the rims of large inclusions.

Mass transfer

For purposes of examining mass transfer between the ultramafic matrix and included lithic-wacke fragments, we calculated cationic proportions from the whole-rock chemical analyses (Table 1) based on 160 oxygen ions per unit cell (Barth, 1948); Table 7 lists the results. Assuming that 160 oxygen ions describe a fixed volume regardless of cationic composition, the number of cations increases across the sequence from 89.2 cations/160 oxygen ions in unaltered lithic wacke to 115 cations/160 oxygen ions in the uncontaminated ultramafic host.

Table 6. Electron microprobe analyses of sheet-silicate phases in lithic-wacke country rock and inclusions

	Muscovite	Chlorite	Biotite(?) remnant	Yellow phase	Stilpnomelane-like phases			Stilpno- melane*
	CYP4	CYP4	CYP4	CYP178	CYP101	CYP7	CYP7	
SiO ₂	49.1	25.3	32.3	33.8	55.6	49.9	49.9	44.52
TiO ₂	0.50	0.03	1.00	0.36	0.00	0.00	0.00	0.10
Al ₂ O ₃	26.2	21.1	16.9	16.4	1.26	0.58	0.58	7.19
FeO ^I	4.47	27.1	23.8	24.0	17.9	16.4	12.8	27.86
MnO	0.00	1.20	0.28	0.20	0.32	0.17	0.29	0.42
MgO	2.56	13.5	12.0	11.3	8.89	7.94	10.0	5.63
CaO	0.00	0.00	0.23	1.05	1.18	7.31	7.23	0.23
Na ₂ O	0.08	0.05	0.11	0.18	2.34	0.04	0.06	0.32
K ₂ O	11.3	0.00	1.92	0.07	2.29	0.00	0.00	1.77
F	0.20	0.09	0.15	0.00	0.02	0.00	0.00	—
Total	88.37	94.41	87.69	87.36	89.80	82.34	80.96	88.04

*Deer et al. (1962, p. 109, table 20, Analysis 9).

Table 7. Cations per 160 oxygen ions for lithic-wacke country rock, lithic-wacke inclusions, augite rinds, and ultramafic host

	Lithic-wacke country rock	Inclusion (6x8 cm)		Inclusion rim	Inclusions (2x3 cm)		Augite rind	Ultramafic host
	CYP4	CYP101A	CYP101B	CYP102B	CYP8	CYP103	CYP8	CYP5
Si	61.0	56.5	57.7	56.7	57.2	57.4	53.1	36.6
Al	13.4	17.6	17.5	17.2	17.0	16.3	0.63	12.0
Fe ³⁺	1.03	1.28	1.19	1.40	1.87	2.21	1.60	6.41
Fe ²⁺	2.37	1.36	1.18	1.71	0.36	0.66	7.79	5.79
Mg	2.34	1.77	2.06	2.71	1.75	2.57	18.4	15.2
Ca	0.36	1.76	1.61	2.78	1.48	0.33	21.4	22.1
Na	7.29	7.78	5.37	4.95	6.28	6.54	2.86	9.95
K	0.90	9.20	13.2	13.2	14.1	14.7	---	2.18
Ti	0.39	0.38	0.33	0.37	0.30	0.30	0.58	2.55
P	0.09	0.08	0.08	0.10	0.02	0.02	---	1.82
Mn	0.04	0.05	0.04	0.04	0.02	0.04	0.31	0.28
Ba	0.02	0.05	0.03	0.01	0.02	0.03	---	0.07
Sum	89.23	97.81	100.29	101.17	100.40	101.10	106.67	114.95

There are exceptionally large contrasts in Si, Ca, Mg, Fe²⁺, Fe³⁺, Ti, and P contents between unaltered lithic wacke and the ultramafic host. As Si was lost from the lithic-wacke fragments to the strongly silica-undersaturated ultramafic melt, K "flooded" the inclusions due to its high activity in that melt. Recall that stable K-bearing phases in sample CYP5 (and other samples of the uncontaminated host) are phlogopite (average X_{phlog} , 0.85) and nepheline containing about 7 wt.% K₂O (approximately Ne₇₅Ks₂₅). Additional indication of high K activity in the ultramafic host is the occurrence of late-stage K-Fe sulfide minerals (Czamanske et al., 1978, 1979, 1981). Loss of Si also may be largely responsible for the apparent increase in the cationic concentration of Al in the inclusions; the resulting average Si/Al of 3.3 approaches the value of 3.0 characteristic of alkali feldspar. The monomineralic augite rind that developed along the contacts of inclusions with the ultramafic magma concentrated Ca, Mg, and Fe²⁺ relative to the lithic wacke, and Mg and Fe²⁺ relative to the ultramafic host. Growth of this rind was promoted by movement of Si from the inclusions outward toward the undersaturated matrix.

Metasomatic reaction caused little change in the cationic contents of Fe, Mg, Ti, Mn, and P within the inclusions, despite large gradients in concentration against the ultramafic melt. Ca-cationic content increased slightly, whereas Na content decreased, a relation suggesting that all the Na from exchanged albite was not fixed locally in new phases. The steady increase in Fe³⁺/(Fe³⁺ + Fe²⁺) with the progression unaltered lithic wacke-inclusion cores-inclusion rims-small inclusions (Table 7) is ascribed to coupling of Fe³⁺ with Na⁺ released from feldspar. Whole-rock data listed in Table 1 show that H₂O was lost and F gained during metasomatism of the inclusions. The amphibole data suggest that F activity was initially high and then declined.

Although the flux of components across the in-

clusion/ultramafic melt interface may have been influenced by the intervening augite rind, chemical variation within coexisting phases in the rim assemblage suggests that the various mineral species crystallized in micro-environments of rapidly changing chemical potentials and intensive parameters. Whereas the augite of the rind crystallized with an essentially fixed Fe/Mg, the sodic pyroxene, in which substitutions involving Na, Ti, and Fe³⁺ are important, became depleted in Ti and enriched in the acmite end member during crystal growth (Table 2). In contrast, early-formed, F-rich richterite evolved to later-crystallizing low-F magnesio-arfvedsonite, enriched in Ti and containing as much as twice the amount of Fe found in the richterite.

A dynamic redistribution of alkalis among coexisting phases has occurred within the inclusions. Alkali feldspar of subequal Na and K contents in the inclusion cores has developed from nearly pure albite and evolved, toward the inclusion/ultramafic interface, first to grains composed of K-rich rims on cores with Na ≈ K, and finally to pure K-feldspar (microcline) grains. Amphibole crystals have cores in which Na/Ca = 1 in the M(4) site and rims in which Na/Ca = 2 in M(4); in sample CYP8, A-site Na is also more abundant in the rims than in the corresponding cores. Na released from alkali feldspar is also found in acmite (of fixed maximum Na content) and in the natrolite-like zeolite phase. These coexisting newly formed Na-rich phases are undersaturated in Si.

It is difficult to know over what range of temperature the redistribution of alkalis took place. The study of Zyrianov et al. (1978) indicates that relatively low K/(K + Na) in aqueous chloride solutions in equilibrium with nepheline can produce K-rich feldspars. At 0.1 GPa, as temperatures fall to 400°C, essentially pure microcline will coexist with Ne₈₈ if K/(K + Na) is greater than about 0.3.

Viewed slightly differently, the replacement of albite by microcline plus Na-rich zeolites in a nepheline-bearing

system may be related to relative desilication reaction stability. Carmichael et al. (1970) considered the relations of albite, orthoclase, nepheline, and leucite in igneous rocks. Carmichael et al. and Baker et al. (1964) proposed on the basis of field observation that the desilication steps of the CIPW-norm calculation are faulty with regard to albite and orthoclase and that "The desilication of orthoclase should precede that of albite..." (Carmichael et al., 1970, p. 246). Our observations indicate that in the significantly different environment of diatreme metasomatism, their proposal is not substantiated. In comparison with K, Na is more adaptable in readily entering pyroxenes, amphiboles, and zeolites in substantial concentrations.

Discussion

Our interpretation is that present exposures were within 1 km of the surface at the time of dynamic eruption of a gas-charged highly fluidized silicate melt. Indications of auto-brecciation and strong chemical disequilibrium on thin-section and hand-specimen scales are ubiquitous features of the diatreme, which has nonetheless solidified to form an impressively unaltered, tough, and compact rock. Poorly consolidated fragmental rocks, as well as the H₂O- and CO₂-rich alteration facies of "typical" ultramafic diatremes, are not found.

The challenge in studying the lithic-wacke inclusions is to interpret mineral relations that have developed at less than 0.1 GPa pressure during exposure to an extremely high temperature event of minimal duration. It is surely relevant that notable mafic phases in vesicles and pumice lapilli in peralkaline silicic welded tuffs are acmite, richterite, and arfvedsonite. Schmincke (1969, 1974), in describing the transition in cooling unit E on Gran Canaria from white to blue-gray (oxidized to reduced), noted a change in the mafic-mineral assemblage from dominant titaniferous acmite to "dominant richterite zoned outward to arfvedsonite(?)."

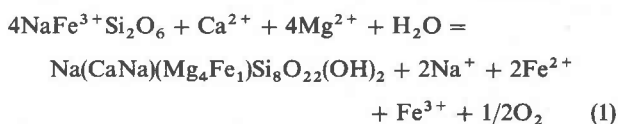
Several excellent experimental and crystal-chemical studies of sodic pyroxenes and alkali amphiboles provide a challenging matrix of information to which our mineralogic data can be related. The system at Coyote Peak was dynamic, and prograde mineral assemblages were typically "frozen" by reaction kinetics as temperatures fell quickly (we find no evidence of retrograde reaction among phases in the ultramafic host or within the lithic-wacke inclusions). Study of thin sections shows that, in comparison with the alkali amphibole, sodic pyroxene stability extended farther into the inclusions. Myriads of fine subhedral to euhedral crystals (typically smaller than 50 μ m) scattered throughout the rock remind one of experimental-run products (Figs. 2B through 2F). In contrast, the alkali amphibole, which appears to have crystallized later, occurs as rather widely separated larger (maximum 1.25 mm across) crystals (Figs. 2D and 2E) within 10 mm of the interface between inclusion and ultramafic host. Amphibole grains are typically free of inclusions but are commonly intergrown with sodic pyroxene along their margins.

The paragenetic relations of sodic pyroxene and am-

phibole, and the zoning of these phases with respect to Ti, are intriguing problems. In terms of bulk composition (Table 1) or cations/160 oxygen ions (Table 7), there is no indication of enrichment in Ti or Na during metasomatism. Most of the arguments of Verhoogen (1962) pertaining to the Ti content of Mg-Fe pyroxenes are contradicted by our data for Na-rich pyroxenes. Figure 4 shows that the titanian component of the Coyote Peak pyroxene cores may be the highest yet observed, and a remarkable aspect of the sodic pyroxenes at Coyote Peak is that their zoning is opposite to that of most known instances of titanian zoning in acmitic pyroxenes. Only Ronsbo et al. (1977) mentioned a few grains of titanian acmite zoned toward colorless acmite from Tertiary ash layers in Denmark. Consideration of Table 2 shows that Ti content is not significantly related to any variables other than the concentration and oxidation state of Fe (Fig. 3).

At least two explanations or a combination thereof may be offered for the atypical Ti zonation in the sodic pyroxenes. It could reflect (1) "capture" of Ti by the first-crystallizing pyroxene or (2) the fact that incorporation of Ti⁴⁺ into sodic pyroxenes is favored by relatively high f_{O_2} . The first explanation merits consideration because the pyroxene-stability field is approached from the low-temperature side in the lithic-wacke inclusions, whereas "... the constant association of late-stage titanian-acmite forming after acmite..." (Ferguson, 1977, p. 248) is created in an environment of falling temperature in which the activity of Ti⁴⁺ may be increasing. However, both this more typical, late-stage environment and the earliest condition within the inclusions are likely to be characterized by the highest f_{O_2} —hence our second explanation. Both Verhoogen (1962) and Flower (1974) emphasize that relatively high f_{O_2} favors incorporation of Ti into pyroxene structures, and natural occurrences of titanian acmite can be interpreted to reflect highly oxidizing environments.

Based on the experimental work of Ernst (1962, Fig. 11), we suggest that the apparent precedence of sodic pyroxene crystallization depended principally on relatively high f_{O_2} inherent to the lithic-wacke inclusions. An electrochemically balanced reaction between acmite and richterite.



shows this relation and illustrates that widespread acmite crystallization also may have been promoted by the first flush of Na⁺ from albite exchange. Although it might be argued that alkali-amphibole crystallization was delayed by relatively late influx of Ca²⁺ and Mg²⁺ from the ultramafic host, we have shown in Table 7 and in our earlier discussion that this seems unlikely. Conceivably, the later and more widely spaced crystallization of amphibole may also partly reflect relative ease of crystallization (Goldsmith, 1953).

The excellent experimental studies of Ernst (1962), Huebner and Papike (1970), and Charles (1974, 1975, 1977),

allow discussion of alkali-amphibole stability relations. The nearly full and relatively constant A-site occupancy in the Coyote Peak amphiboles agrees with their stability at relatively low pressure and high temperature (Forbes, 1971; Charles, 1975). Moreover, the chemical environment within the inclusion is fully compatible with the statement of Huebner and Papike (1970, p. 1973) that "The formula further suggests that richterite crystallizes in an environment in which the chemical potential of alkalis is great relative to that of alumina." (See also Charles, 1977, p. 621).

Charles (1977, Fig. 1) showed that richterite of the composition of the Coyote Peak amphibole cores, approximately Mg_4Fe , is stable at quite low f_{O_2} (e.g., 10^{-21} at 600°C and 0.1 GPa on the quartz-fayalite-magnetite buffer). Ernst (1962, p. 732) found similar stability limits for arfvedsonite and concluded that "Arfvedsonite-bearing assemblages are presumed to have crystallized at lower oxidation states..." Presumably, substitution of Ti^{4+} for Fe^{3+} in the arfvedsonitic rims of the Coyote Peak amphiboles may be compatible with even lower f_{O_2} . These and other important reactions involving amphiboles and biotite were thoroughly discussed by Wones (1981).

We envision that the lithic-wacke inclusions reached some maximum temperature quickly and then recrystallized over a somewhat longer, but still relatively short, time interval. As K displaced Na from feldspar and inherent f_{O_2} was high due to the presence of detrital hydrous and oxidized phases, abundant acmite crystallized. With falling T and f_{O_2} , richterite, further stabilized by F, began to form more widely spaced crystals. Absence of acmite crystals within relatively larger, contiguous amphibole grains can be understood by consideration of reaction (1), which suggests that acmite could react readily to form sodic amphibole. As T and f_{O_2} continued to decrease, titanian arfvedsonite supplanted richterite as the stable phase, and zoned alkali-amphibole grains were formed.

Acknowledgments

We appreciate the assistance of Richard C. Erd and Gordon Nord with the X-ray diffraction and transmission microscope studies. Thoughtful reviews by Jane Hammarstrom, Tren Haselton, Stephen Huebner, Malcolm Ross, Donald Voight, and David Wones helped to clarify our presentation.

References

- Bailey, E. H., Irwin, W. P., and Jones, D. L. (1964) Franciscan and related rocks and their significance in the geology of western California. California Division of Mines and Geology, Bulletin 183.
- Baker, P. E., Gass, I. G., Harris, P. G., and LeMaitre, R. W. (1964) The volcanological report of the Royal Society expedition to Tristan da Cunha. Royal Society, London, Philosophical Transactions, 256, Series A, 439-578.
- Barth, T. F. W. (1948) Oxygen in rocks: a basis for petrographic calculations. *Journal of Geology*, 56, 50-60.
- Cameron, M. and Gibbs, G. V. (1973) The crystal structure and bonding of fluor-tremolite: a comparison with hydroxyl tremolite. *American Mineralogist*, 58, 879-888.
- Cameron, M. and Papike, J. J. (1981) Structural and chemical variations in pyroxenes. *American Mineralogist*, 66, 1-50.
- Carmichael, I. S. E., Nicholls, J., and Smith, A. L. (1970) Silica activity in igneous rocks. *American Mineralogist*, 55, 246-263.
- Charles, R. W. (1974) The physical properties of the Mg-Fe richterites. *American Mineralogist*, 59, 518-528.
- Charles, R. W. (1975) The phase equilibria of richterite and ferro-richterite. *American Mineralogist*, 60, 367-374.
- Charles, R. W. (1977) The phase equilibria of intermediate compositions on the pseudobinary $Na_2CaMg_5Si_8O_{22}(OH)_2$ - $Na_2CaFe_5Si_8O_{22}(OH)_2$. *American Journal of Science*, 277, 594-625.
- Czamanske, G. K. and Wones, D. R. (1973) Oxidation during magmatic differentiation, Finnmarka complex, Oslo area, Norway: Part II, The mafic silicates, *Journal of Petrology* 14, 349-380.
- Czamanske, G. K., Meyer, C. E., Erd, R. C., and Norman, M. B., II (1977) The Coyote Peak diatreme, Humboldt County, California (abstr.). *EOS*, 58, 1247.
- Czamanske, G. K., Erd, R. C., Sokolova, M. N., Dobrovolskaya, M. G., and Dmitrieva, M. T. (1979) New data on rasvumite and djerfisherite. *American Mineralogist*, 64, 776-778.
- Czamanske, G. K., Leonard, B. F., and Clark, J. R. (1980) Erdite, a new hydrated sodium iron sulfide mineral. *American Mineralogist*, 65, 509-515.
- Czamanske, G. K., Erd, R. C., Leonard, B. F., and Clark, J. R. (1981) Bartonite, a new potassium iron sulfide mineral. *American Mineralogist*, 66, 369-375.
- Deer, W. A., Howie, R. A., and Zussman, J. (1962) *Rock-forming Minerals*, Vol. 3, Sheet silicates, Longman, London.
- Deer, W. A., Howie, R. A., and Zussman, J. (1978) *Rock-forming Minerals*, Vol. 2A, Single-chain silicates. John Wiley and Sons, New York.
- Erd, R. C. and Czamanske, G. K. (1983) Orickite and coyoteite, two new sulfide minerals from Coyote Peak, Humboldt County, California. *American Mineralogist*, 68, 245-254.
- Ernst, W. G. (1962) Synthesis, stability relations, and occurrence of riebeckite and riebeckite-arfvedsonite solid solutions. *Journal of Geology*, 70, 689-736.
- Ernst, W. G. (1965) Mineral parageneses in Franciscan metamorphic rocks, Panoche Pass, California. *Geological Society of America Bulletin*, 76, 879-914.
- Ferguson, A. K. (1977) The natural occurrence of aegirine-neptunite solid solution. *Contributions to Mineralogy and Petrology*, 60, 247-253.
- Flower, M. F. J. (1974) Phase relations of titan-acmite in the system Na_2O - Fe_2O_3 - Al_2O_3 - TiO_2 - SiO_2 at 1000 bars total water pressure. *American Mineralogist*, 59, 536-548.
- Forbes, W. C. (1971) Synthesis and stability relations of richterite. *American Mineralogist*, 56, 997-1004.
- Ghose, S. (1965) A scheme of cation distribution in the amphiboles. *Mineralogical Magazine*, 35, 46-54.
- Goldsmith, J. R. (1953) A "simplicity principle" and its relation to "ease" of crystallization. *Journal of Geology*, 61, 439-451.
- Grapes, Rodney, Yagi, Kenzo, and Okumura, Kimio (1979) Aenigmatite, sodic pyroxene, arfvedsonite and associated minerals in syenites from Morotu, Sakhalin. *Contributions of Mineralogy and Petrology*, 69, 97-103.
- Hawthorne, F. C. (1981) Crystal chemistry of the amphiboles. In D. R. Veblen, Ed., *Amphiboles*, Reviews in Mineralogy, vol. 9A, p. 1-102. Mineralogical Society of America, Washington, D. C.
- Huebner, J. S. and Papike, J. J. (1970) Synthesis and crystal chemistry of sodium-potassium richterite (Na,K)NaCaMg,

- $\text{Si}_8\text{O}_{22}(\text{OH},\text{F})_2$: A model for amphiboles. *American Mineralogist*, 55, 1973–1992.
- Kitamura, M., Tokonami, M., and Morimoto, N. (1975) Distribution of titanium atoms in oxy-kaersutite. *Contributions to Mineralogy and Petrology*, 51, 167–172.
- Leake, B. E. (1978) Nomenclature of amphiboles. *Canadian Mineralogist*, 16, 501–520 (Also *American Mineralogist*, 63, 1023–1052).
- Morgan, J. W., Czamanske, G. K., and Wandless, G. A. (1985) Origin and evolution of the alkalic ultramafic rocks in the Coyote Peak diatreme, Humboldt County, California. *Geochimica et Cosmochimica Acta*, 49, 749–760.
- Nielsen, T. F. D. (1979) The occurrence and formation of Ti-aegirines in peralkaline syenites. *Contributions to Mineralogy and Petrology*, 69, 235–244.
- Papike, J. J., Ross, M., and Clark, J. R. (1969) Crystal-chemical characterization of clinoamphiboles based on five new structure refinements. *Mineralogical Society of America, Special Paper 2*, 117–136.
- Papike, J. J., Cameron, K. L., and Baldwin, K. (1974) Amphiboles and pyroxenes: characterization of other than quadrilateral components and estimates of ferric iron from microprobe data. *Geological Society of America, Abstracts with Programs 6*, 1053–1054.
- Robinson, Peter (1980) The composition space of terrestrial pyroxenes—internal and external limits. In C. T. Prewitt, Ed., *Pyroxenes, Reviews in Mineralogy*, vol. 7, p. 419–494. *Mineralogical Society of America, Washington, D. C.*
- Ronsbo, J. G., Pedersen, A. K., and Engell, J. (1977) Titan-aegirine from early Tertiary ash layers in northern Denmark. *Lithos*, 10, 193–204.
- Rosenberg, P. E., and Foit, F. F., Jr. (1977) Fe^{2+} —F avoidance in silicates. *Geochimica et Cosmochimica Acta*, 41, 345–346.
- Scheumann, K. H., 1913, *Petrographische Untersuchungen an Gesteinen des Polzengebietes in Nord Böhmen; insbesondere über die Spaltungsserie der Polzenit-Trachydolerit-Phonolith-Reihe*, in *Der Abhandlungen der mathematisch-physischen Klasse der Königl. Sächsischen Gesellschaft der Wissenschaften*: Leipzig, B. G. Teubner, v. 32, no. 7, p. 759.
- Schmincke, H.-U. (1969) Ignimbrite sequence on Gran Canaria. *Bulletin Volcanologique*, 33, 1199–1218.
- Schmincke, H.-U. (1974) Volcanological aspects of peralkaline silicic welded ash-flow tuffs. *Bulletin Volcanologique*, 38, 594–636.
- Scott, P. W. (1976) Crystallization trends of pyroxenes from the alkaline volcanic rocks of Tenerife, Canary Islands. *Mineralogical Magazine*, 40, 805–816.
- Verhoogen, J. (1962) Distribution of titanium between silicates and oxides in igneous rocks. *American Journal of Science*, 260, 211–220.
- Whittaker, E. J. W. (1949) The structure of Bolivian crocidolite. *Acta Crystallographica*, 2, 312–317.
- Whittaker, E. J. W. (1960) The crystal chemistry of the amphiboles. *Acta Crystallographica*, 13, 291–298.
- Whittaker, E. J. W. and Muntus, R. (1970) Ionic radii for use in geochemistry. *Geochimica et Cosmochimica Acta*, 34, 945–956.
- Wones, D. R. (1981) Mafic silicates as indicators of intensive variables in granitic magmas. *Mining Geology [Society of Mining Geologists of Japan]* 31(4), no. 168, 191–212.
- Yakowitz, H., Myklebust, R. L., and Heinrich, K. F. J. (1973) FRAME: An on-line correction procedure for quantitative electron probe analyses. *National Bureau of Standards Technical Note 796*.
- Zyrianov, V. N., Perchuk, L. L., and Podlesskii, K. K. (1978) Nepheline—alkali feldspar equilibria: I. Experimental data and thermodynamic calculations. *Journal of Petrology*, 19, 1–44.

*Manuscript received, September 6, 1983;
accepted for publication, January 14, 1985.*